Palaeogeography, Palaeoclimatology, Palaeoecology 299 (2011) 200–213

Contents lists available at ScienceDirect

Palaeogeography, Palaeoclimatology, Palaeoecology

journal homepage: www.elsevier.com/locate/palaeo

# The Permian Moradi Formation of northern Niger: Paleosol morphology, petrography and mineralogy

Neil J. Tabor [a,*], Roger M.H. Smith [b], J. Sébastien Steyer [c], Christian A. Sidor [d], Christopher J. Poulsen [e]

[a] Roy M. Huffington Department of Earth Sciences, 3225 Daniel Avenue, Dallas, TX 75275-0395, United States
[b] Division of Earth Sciences, Iziko: South African Museum, Cape Town 8000, South Africa
[c] CNRS UMR7207, Muséum national d'Histoire naturelle, Département Histoire de la Terre, CP38, 8 rue Buffon, F-75005 Paris cedex 05, France
[d] Burke Museum and Department of Biology, University of Washington, Seattle, WA 98195-1800, United States
[e] Department of Geological Sciences, University of Michigan, Ann Arbor, MI 48109, United States

ARTICLE INFO

*Article history:*
Received 20 April 2010
Received in revised form 11 October 2010
Accepted 1 November 2010
Available online 4 November 2010

*Keywords:*
Paleosols
Clay mineralogy
Paleoclimate
Permian
Moradi Formation
Niger
Africa

ABSTRACT

Three basic paleosol morphologies, named Type A, Type B and Type C, are described from the middle–upper Permian strata of the Moradi Formation, Tim Mersoi Basin, northern Niger. The Moradi Formation is a typical alluvial redbed succession dominated by red mudrocks with fine to coarse-grained pebbly channel sandstones and matrix-breccias. Type A paleosols are hosted by well-sorted fine to medium grained trough cross bedded and massive sandstones and preserve abundant vertical to horizontal micritic and microspar calcite tubules, interpreted as rhizoliths. Lateral variability of rhizoliths in Type A paleosols, and their close association with fluvial channel-fill sediments suggests they are the roots of grove stands of phreatophytic vegetation that grew within unstable anabranching stream systems. Type B paleosols are hosted by mudrocks and preserve well-developed ped structure, abundant micritic calcite nodules and vertically-stacked micritic calcite nodular bodies, as well as rare calcite with satin-spar texture interpreted as a pseudomorphic replacement of pedogenic gypsum. The morphology of Type B paleosols suggests they were formed in well-drained floodplain deposits on stable landforms. Type C paleosols are similar to Type B but preserve pedogenic structures indicative of soil volume expansion and contraction, as well as more abundant Stage II pedogenic carbonate nodules. The morphology of Type C paleosols suggests that they developed periodically rather than seasonally in poorly-drained deposits that nevertheless occupied a relatively stable part of the landscape such as the plains flanking ephemeral lakes or sabkhas.

X-ray diffraction analysis of the <2 μm fraction from the Moradi Formation strata indicates that paleosol phyllosilicates are composed of illite, smectite, and occasionally kaolinite and talc. Illite is likely a detrital mineral, whereas smectite and kaolinite are likely pedogenic weathering products. The presence of talc in the Moradi Formation paleosols is unusual. It is limited to paleosol horizons that also preserve evidence for pedogenic gypsum accumulation and is therefore most likely related to a pedogenic weathering process. It is possible that this talc is a relatively low-temperature (~50–100 °C) diagenetic alteration product of pedogenic Mg–phyllosilicates such as sepiolite.

The range of morphologies, petrographic textures and mineralogy of the paleosol profiles indicates semi-arid to hyper-arid climatic setting. This paleoclimatic reconstruction is in agreement with Middle and Late Permian conceptual paleoclimate models and quantitative general circulation models. Nevertheless, and in spite of an arid climate, Moradi paleosols and their host strata also indicate a relatively shallow groundwater table. Importantly, this shallow groundwater resource undoubtedly helped to support the moderately diverse fossil vertebrate assemblage and large-stature macrophytes preserved in the Moradi Formation.



## 1. Introduction

The past few decades have seen significant advances in understanding of Permian terrestrial climate evolution across northern mid-latitude (Newell et al., 1999; Rees et al., 2002; Yakimenko et al., 2004), equatorial (e.g. DiMichele et al., 2009; Nairn and Smithwich, 1976; Parrish, 1982, 1993; Schneider et al., 2006; Steel, 1974; Tabor et al., 2007; Tramp et al., 2004; Ziegler et al., 1997, 2003) and extreme southern mid-latitude and polar landscapes (Fielding et al., 2008; Isbell et al., 2003; Retallack et al., 2003; Smith, 1990; Wopfner, 2002; Wopfner and Kreuser, 1986). Permian climate history from south-central Pangean regions, including sub-Saharan Africa and northern South America (Fig. 1A), remains especially poorly known (e.g., Rees

* Corresponding author.
*E-mail addresses:* ntabor@mail.smu.edu (N.J. Tabor), rsmith@iziko.co.za (R.M.H. Smith), steyer@mnhn.fr (J.S. Steyer), casidor@uw.edu (C.A. Sidor), poulsen@umich.edu (C.J. Poulsen).

0031-0182/$ – see front matter © 2010 Elsevier B.V. All rights reserved.
doi:10.1016/j.palaeo.2010.11.002

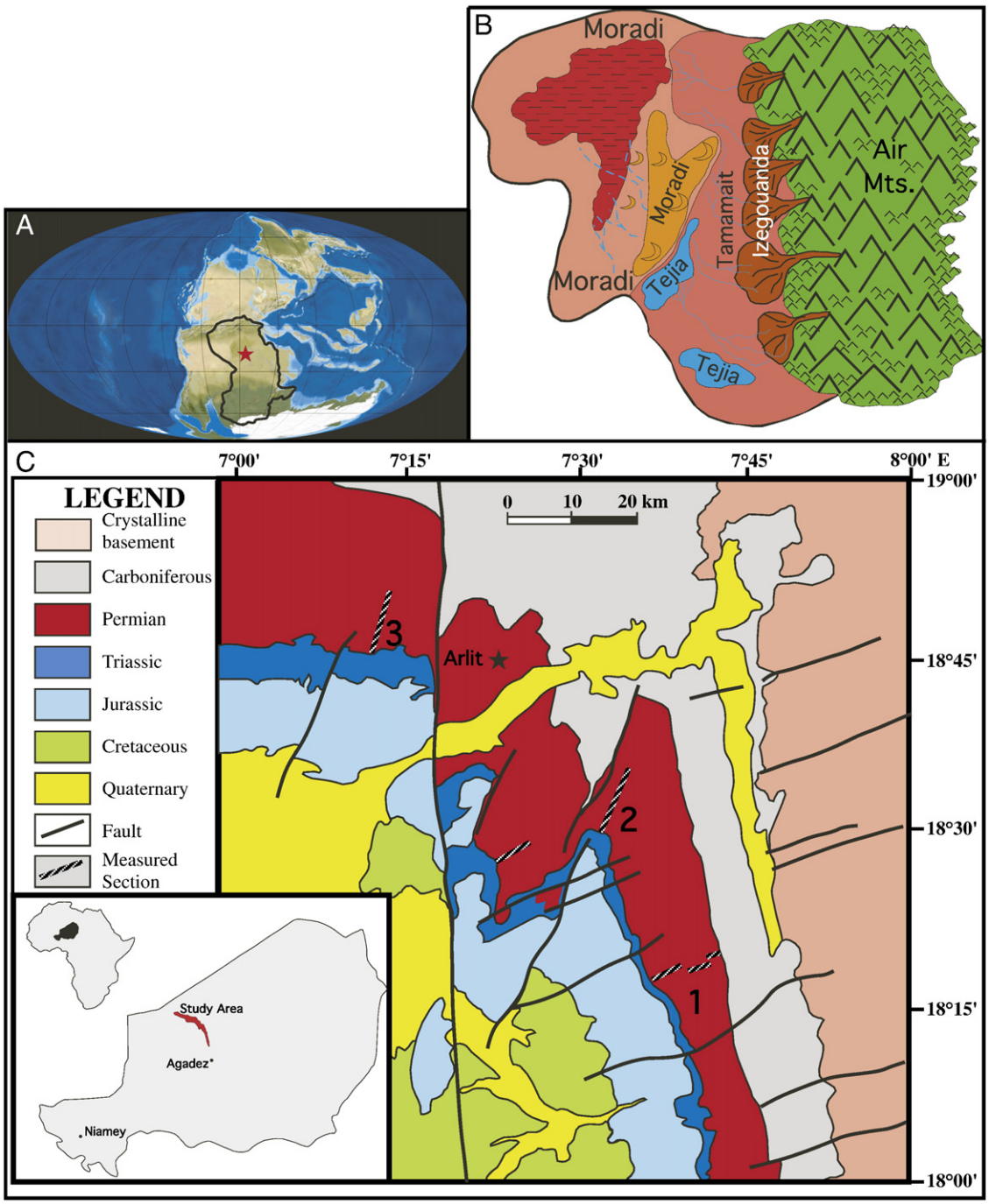


**Fig. 1.** Generalized geography of the study area. (A) Paleogeographic reconstruction of Permian Earth (~260 million years ago; after Blakey, 2007). Lines of longitude and latitude are separated by 30°. The borders of the African tectonic plate are outlined. A red star marks the approximate paleogeographic position of the Tim Mersoi Basin during Middle Permian time (~260 Ma). (B) Regional landscape reconstruction of the Tim Mersoi Basin (after Wright et al., 1993). The Aïr Mountains were a positive topographic feature and were responsible for delivery of coarse sediments along the eastern portion of the Tim Mersoi Basin (see text). Particular facies in this reconstruction are attributed to entire formations within the Permian strata of the Tim Mersoi Basin. While such an attribution is a suspect, this image nevertheless provides a reasonable representation of the physiography of the Tim Mersoi Basin during Permian deposition. (C) Geologic map of the field study areas. Black star marks the nearby town of Arlit. Solid black lines depict significant fault displacements; note that the majority of faults cut Cretaceous and Quaternary strata, and therefore most brittle deformation of the Tim Mersoi Basin likely occurred during Cenozoic time. Hatched black lines, numbered 1, 2, and 3 depict the location of measured stratigraphic sections referred to throughout the text.

et al., 2002; Ricardi-Branco, 2008) in large part because of a paucity of Permian-age sedimentary rocks in the region. Therefore, the few basins that are known to have occupied south-central Pangea with outcrops that contain sedimentary and biological records of Permian time are critically important for paleoclimate studies. They provide the only geologically-based proxy data for paleoclimate reconstructions, they help to fill the spatial and temporal knowledge gap that exists between the Permian tropics and southern high-latitudes, and they provide the "ground-truth" needed to test, modify and refine conceptual and quantitative paleoclimate models.

The results from study of alluvial paleosol profiles preserved within the Permian Moradi Formation of the Tim Mersoi Basin, Niger are presented herein. Field-scale observations of paleosol morphology, in conjunction with petrographic and mineralogical analyses

provide, for the first time, geologically-based proxy data for paleoclimate from south-central Pangea.

## 2. Geological background

Middle and Upper Permian rocks of the Tim Mersoi sub-basin of the Iullemeden basin are exposed in a southwest-northeast outcrop belt in north-central Niger (Greigert and Pougnet, 1967; Kogbe, 1981; Fig. 1). The tectonic setting of this basin is not well understood, although it has been proposed that compressional forces resulting from late Paleozoic collision of Gondwana and Laurasia caused reactivation of strike slip faults in the Pre-Cambrian basement, uplift of the Aïr Massif, and down warping of adjacent crust. Elevated fault scarps associated with the paleo-Aïr highlands sourced numerous rivers that flowed west and north into the closed continental Tim Mersoi basin in which the sediments of the Permian Izegouandane Group accumulated (Sidor et al., 2005; Figs. 1 and 2).

Upper Paleozoic strata in Niger have been only superficially described (Greigert and Pougnet, 1967; Joulia, 1959; Ministère des Mines et de l'Hydraulique, 1977; Trompette et al., 1980; Wright et al., 1993). The Izegouandane Group is composed of up to ~250 m of nonmarine detrital siliciclastic strata that are subdivided into four conformable formations: the lowermost sandstone-dominated Izégouandane, mudstone-dominated Tejia, sandstone-dominated Tamamaït, and the uppermost Moradi (Fig. 2B and C). The Moradi Formation consists dominantly of red mudstones with secondary fluvial channel sandstones

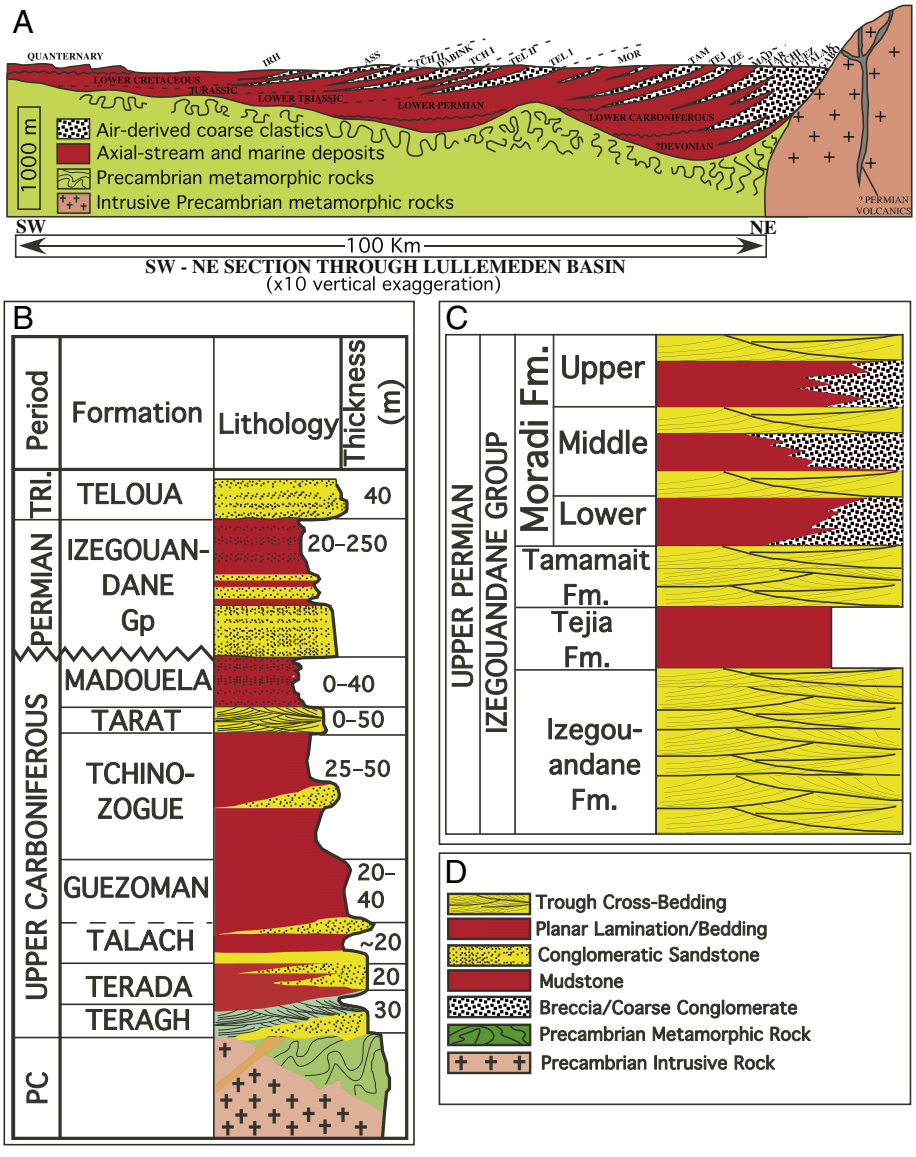


**Fig. 2.** Generalized geology of northern Niger. (A) Geological cross section of the greater Iullumeden Basin, which includes the northern Tim Mersoi Basin. This basin preserves Devonian- through Quaternary-age sediments that rest nonconformably upon Precambrian metamorphic rocks. All strata in the basin, except Quaternary, exhibit structural dips toward the west-southwest that are slight (~1°) in the west and more extreme (up to 15°) in the eastern part of the basin. Structural relationships indicate that the Aïr Mountains have been the eastern boundary of this basin since at least Early Carboniferous time, and that vertical motions of the Aïr intermittently delivered coarse clastic materials westwards. Away from the Aïr Mountains, the sedimentary rocks are dominated by fluviatile and marine strata. Lithological units are noted above the cross section: GABO = equivalent to Terada and Teragh formations in Fig. 4B, TALAK = Talach Formation, GUEZ = Guezoman Formation, TCHI = Tchinozogue Formation, TAR = Tarat Formation, MAD = Madouela Formation, IZE = Izegouandane Formation, TEJ = Tejia Formation, TAM = Tamamait Formation, MOR = Moradi Formation, TEL I and TEL II = Teloua Formation, TCH I = lower Tchirezrine Formation, DABINK = d'Abinky Formation, TCH II = upper Tchirezrine Formation, ASS = Assaouas Formation, and IRH = Irhazer Formation. The approximate position of fossil-bearing strata in the Moradi Formation is indicated by a bracket. (B) Generalized lithostratigraphy of the Tim Mersoi Basin up to Triassic strata. (C) Generalized stratigraphy of the Permian Izegouandane Group. (D) Legend to the lithostratigraphic symbols used in B and C. See text for details.

and conglomeratic sandstones as well as rare coarse breccias (Fig. 2C). Previous workers in the Moradi Formation have interpreted five depositional facies as (1) minor coarse-grained alluvial fan deposits, (2) common fluvial sandstones deposited in axial streams, (3) common fine-grained overbank/floodplain mudstones, (4) rare fine-grained sabkha mudstones and carbonates and (5) rare eolian sand dunes (Joulia, 1959; Wright et al., 1993). A Middle or Late Permian age of deposition for Izegouandane Group strata is based primarily upon biostratigraphic correlations of fossil vertebrates in the Moradi Formation with Upper Permian vertebrate fossil assemblages in Russia and South Africa (Lucas, 2004; Sidor et al., 2005; Taquet, 1969) as well as by the inferred ages of the underlying Carboniferous and overlying Triassic strata within the Tim Mersoi basin (Ministère des Mines et de l'Hydraulique, 1977; Taquet, 1972). At the time of infilling, this basin was moving northward from ~30 to ~10°S (Scotese et al., 1999), and remained at least 2000 km from the nearest open ocean (Fig. 1).

This work focuses on profile descriptions and sample analyses of paleosols from outcrops comprising lower, middle, and upper parts of the Moradi Formation (Figs. 1C and 3) with a view to gaining further insight into the palaeoclimate that prevailed in continental central Pangea in the Mid to Late Permian.

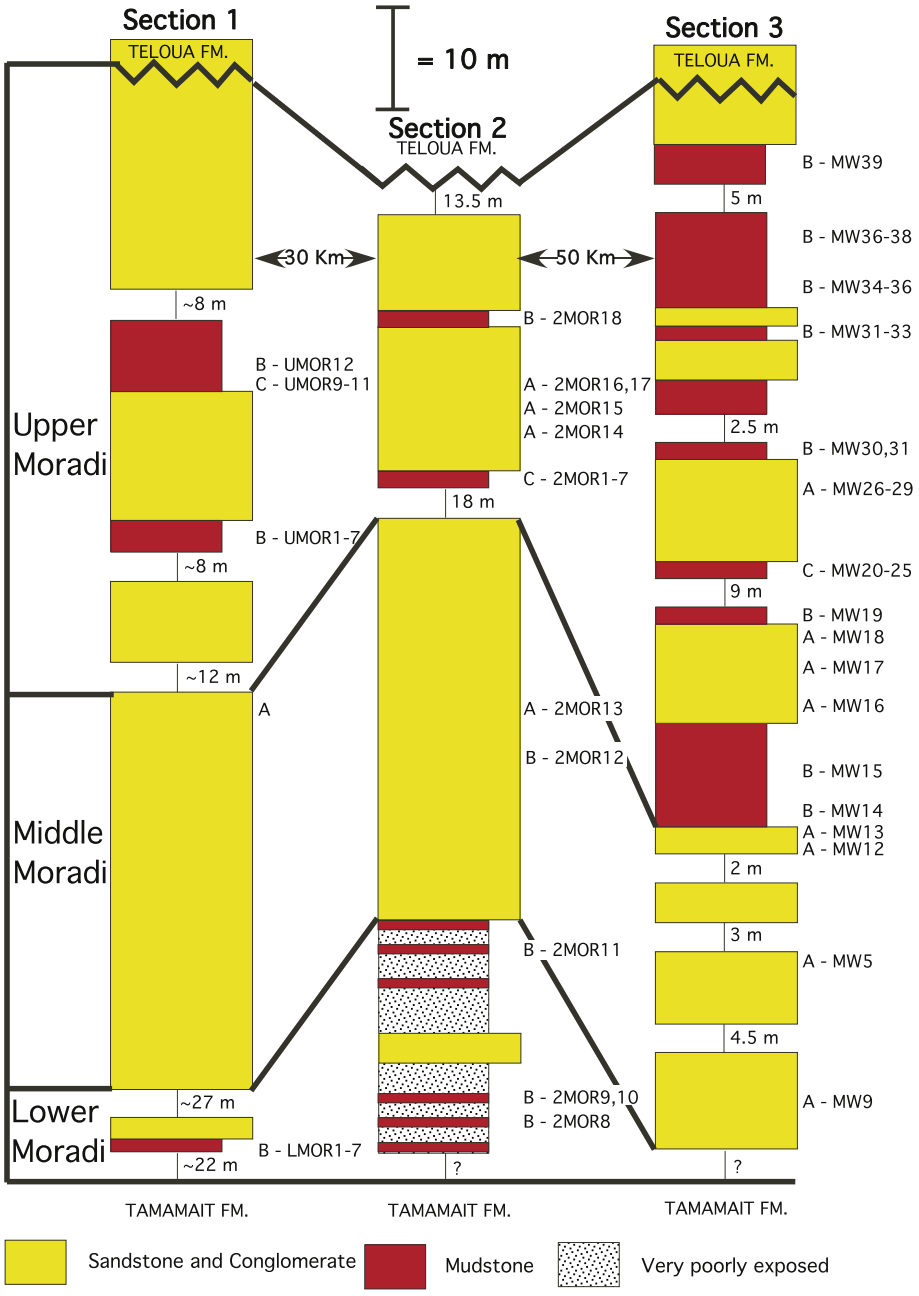


**Fig. 3.** Schematics of measured stratigraphic sections in the Moradi Formation. Section 1, Section 2, and Section 3 are marked in Fig. 1. The scale bar (= 10 m) above Section 2 applies to the vertical scale for measured sandstone and conglomerate (yellow), mudstone (red), and very poorly exposed (stippled) strata. The thin vertical lines connecting yellow and red areas represent covered sections in the Moradi strata; the numbers next to the vertical lines indicate the thickness (in m) of strata that is covered in the section. Thick black lines delimit the boundaries between the Permian Tamamäit Formation, the lower, middle and upper Moradi Formation, and the overlying Triassic Teloua Formation. The text on the right side of each stratigraphic column denotes the location of paleosol profiles in the Moradi Formation stratigraphy. The first letter indicates paleosol type at that location, whereas the number, or number series, after the hyphen indicates the name(s) of sample(s) collected from that site.

## 3. Methods

### 3.1. Field

Although there is very little vegetative cover in the study area, a combination of low-lying topography, low regional dip (<2°) and a modern regolith mantle often exceeding 400 mm thick contributes to a poor quality of surface exposures of Moradi rocks. As a result, the measured stratigraphic sections of the Moradi Formation include numerous covered intervals (Fig. 3), and many parts of the stratigraphy were described from excavation pits up to 1.5 m deep. Moreover, accurate stratigraphic correlation cannot be made between the measured sections (see Fig. 1C). However, a regionally persistent interval of channel sandstones in the middle part of the Moradi Formation (the middle Moradi sands; Fig. 2C) permits general assignment of measured sections to the lower, middle or upper Moradi Formation (Figs. 1C and 3).

Paleopedogenically modified strata were logged and described in detail according to previously defined methods (Tabor and Montañez, 2004; Tabor et al., 2006). The top of each paleosol profile was identified on the basis of a marked change in grain size and color, as well as preservation of primary sedimentary structures. Profile bases were delineated at the re-appearance of unaltered parent material. Paleosol matrix was sampled at 0.1–0.2 m intervals from the top and rhizoliths and paleosol nodules were sampled where present. While modern soil classification schemes have been applied to paleosol profiles (e.g., Blodgett, 1988; Retallack et al., 2003; Tabor and Montañez, 2004), the paleosol classification scheme of Mack et al. (1993) is employed here because it utilizes morphological features that are likely preserved through burial, diagenesis and lithification of a soil profile and is based upon readily observable field properties. The stratigraphic positions and host lithologies of collected samples, are shown in Fig. 3.

### 3.2. Laboratory

Paleosol matrix samples were disaggregated by ultrasonic agitation in a dilute $Na_2CO_3$ solution for 45 min. Thin sections ($n=32$) of representative samples were examined for their micromorphology and mineralogy and described according to the approaches and terminology of Brewer (1976) and Wright (1990).

Whole-rock paleosol matrix and nodule samples were ground in a corundum mortar and pestle and loaded as randomly oriented powder mounts for continuous scan X-ray diffraction analyses using a Rigaku Ultima III X-ray diffractometer with Cu-Kα radiation at a scanning speed of 1° 2θ/min. Carbonate and matrix mineralogy was determined by comparison of X-ray spectra with JCPDS-ICDD standards (1980).

X-ray diffraction of the <2 μm size fraction was carried out for identification of minerals in the clay-size fraction following the methods outlined by Moore and Reynolds (1997). Samples were exchange saturated with $K^+$ or $Mg^{2+}$ on filter membranes and transferred to glass slides as oriented aggregates. A split of the $Mg^{2+}$-saturated clays was also treated with glycerol. Oriented aggregates of all $Mg^{2+}$-treated samples were analyzed at 25 °C. $K^+$-treated samples were analyzed at 25 °C and 500 °C after 2 h of initial heating at their respective temperatures. All X-ray scans of <2 μm samples were performed on a Rigaku Ultima III X-ray diffractometer with CuKα radiation between 2 and 30° 2θ with a step size of 0.04° 2θ and a 1 s count time.

## 4. Results

Paleosol profiles were subdivided into horizons on the basis of down-profile changes in macro- and micromorphological features (Figs. 4 and 5). Three major types of paleosol morphologies (Types A, B and C) exist in the Moradi strata based on the presence of distinctive characteristics that include soil structure, accumulation of carbonate and gypsum, slickensides, fossil root traces and color (Figs. 4 and 5). Later, we first describe the morphology, mineralogy (Fig. 6) and petrography (Fig. 7) of the paleosol profiles. We then discuss the morphological variability among paleosol types, as well as their stratigraphic and lateral distribution within the study area.

### 4.1. Description of Type A paleosols

Type A paleosols exhibit rooting structures and partial to complete obliteration of original depositional features (Figs. 3, 4A,B, and 5). These paleosols exist primarily as pale yellow (Munsell colors 5Y 7/2 to 5Y 8/6), occasionally weak red (Munsell colors 10R 4/3 to 10R 5/4), profiles of well-sorted sandstone, and range from 50 to 250 cm thick. All Type A paleosol profiles exhibit massive structure and/or relict sedimentary structures (e.g., Figs. 4A and 5). The majority of these paleosols preserve tubular gray carbonate concretions ranging from ~1 mm to 100 mm in diameter, and from ~10 mm to 3.7 m in length (Fig. 5A and B). The tubules exhibit a full range of orientations from horizontal to vertical, although all of the tubules within an individual horizon tend to share similar orientations (Fig. 4A). In lateral exposures of Type A paleosols the profiles can be traced in excess of 1.5 km without any significant changes in their overall morphology. However, the abundance of carbonate tubules varies significantly along strike. Laterally extensive outcrops (~10–40 m) preserve tubular carbonate structures that make up to 20–25% of the upper meter in the paleosol profile. These areas of concentrated tubular carbonate are separated by outcrops of 10s to 100s of meters along strike with very few (<2% by volume), or no, carbonate tubules. Type A paleosols have been described in both the middle and upper Moradi Formation; they are limited to very fine to medium sandstones, and are especially common within the upper 1–2 m of thick sandstones that preserve trough cross-strata (Fig. 5).

Petrographic inspection of the sand-rich profiles reveals that Type A paleosols consist of sub-equal amounts of rounded (1) quartz and (2) feldspar grains as well as (3) rounded mud-ball rip-up clasts with disorthic and septarian cracks cemented by sparry carbonate up to 5 mm in diameter, and rounded and elongate clasts of micritic to microspar carbonate (Fig. 7A). In addition, petrographic inspection of the calcareous tubules reveals that they consist primarily of clotted micrite cements organized into a laminar fabric that is intercalated with lenticular domains of microspar to spar cement (Fig. 7B).

X-ray powder diffraction spectra of the sand-rich and muddy sandstone Type A paleosol profiles include major peaks at ~6.4 Å, 3.34 Å and 3.03 Å, which confirms the presence of feldspar, quartz, and low-Mg calcite, respectively (Fig. 6A). In addition, low and broad peaks between ~3 and 10° 2θ indicate the presence of phyllosilicate minerals.

### 4.2. Description of Type B paleosols

Type B paleosol profiles consist of layers of weak red to red (Munsell colors 10R 4/4 to 10R 5/8) mudstones ranging from 0.9 to 3.5 m thick with a fine to coarse blocky ped structure. The upper 50 to 300 mm of these profiles is typically noncalcareous. However, the most obvious feature of these paleosol profiles is an abundance of discrete carbonate nodules, vertically stacked carbonate nodules (*sensu* Blodgett, 1988) and vertically and horizontally orientated carbonate tubules (Fig. 4C). In addition, micro-crystalline calcite is precipitated onto the exterior surfaces of mudstone blocks within the profiles (Fig. 4C) and, in three separate instances, in layers directly beneath nodular carbonate horizons (LMOR1-7, UMOR1-7, MW30-31; Fig. 3), calcareous cements with satin-spar macroscopic fabric line the interstices between mudstone blocks.

Carbonate nodules range from a few mm to ~50 mm in diameter and tend to be concentrated in the lower half of Type B profiles.


**Fig. 4.** Field photographs of paleosols from the Moradi Formation. (A) Trough-cross bedded medium sandstone with abundant, mostly horizontally oriented, calcareous tubules. The hammer is 300 mm long. This outcrop occurs in the upper Moradi Formation near Section 2, at the stratigraphic position of 2MOR15 (see Fig. 3). (B) Close-up photograph of a cross section of a calcareous tubule and sandstone paleosol matrix from the Type A paleosol shown in A. The calcareous tubule mostly excludes sand grains from the paleosol matrix, and exhibits in cross section a laminar to lenticular series of micritic calcite and microspar calcite laminations/lenses. Width of calcareous tubule is 63 mm. (C) Type B paleosol profile from the Upper Permian Moradi Formation. The pencil is 140 mm long. The upper 250 mm of this paleosol profile is shown, and is overlain by a scoured upper boundary and trough-cross bedded mud–pebble conglomerate (upper ~5 cm of photo). This Type B paleosol exhibits medium blocky structure (large mudstone blocks) with secondary fine angular blocky structure (red areas) cemented by microcrystalline calcite (white areas; calcans, Brewer, 1976). This outcrop occurs in the upper Moradi Formation near Section 1, at the stratigraphic position of UMOR1-7 (See Fig. 3). (D) Type C paleosol profile from the Upper Permian Moradi Formation. Paleosol matrix is organized in fine-to-medium wedge-shaped aggregrate structures. Pedogenic slickensides in this paleosol profile are lined by calcite that exhibit satin-spar texture interpreted to have been pedogenic gypsum (gypsans; Brewer, 1976) subsequently recrystallized to calcite. This outcrop occurs in the upper Moradi Formation near Section 3, at the stratigraphic position of MW20-25. Hammer for scale; distance from mid-line of hammer stalk to pick-tip is 114 mm. (E) Type C paleosol profile from upper Moradi Formation. Paleosol matrix (red mudstone) is organized into fine to medium angular peds and fine prismatic peds with microcrystalline calcite cement filling the interstices between mudstone blocks (calcans; Brewer, 1976). Also shown within the paleosol matrix are calcareous nodules and tubules up to 38 mm in diameter/length. This outcrop occurs near Section 3, in the upper horizons of a paleosol profile at the stratigraphic position of 2MOR1-7 (see Fig. 3). See text for discussion.

Stacked nodules and tubules range from ~5 mm to 30 mm in diameter and extend 200 mm to 3.5 m down from profile tops. Two different Type B paleosol profiles in the upper Moradi Formation (MW39, MW36-38; Fig. 3) also preserve siliceous carbonate tubules that range from ~1 mm to 5 mm in diameter, and from ~5 mm to 2.5 m in length as well as silica-rich nodules up to 25 mm in diameter. Type B paleosol profiles commonly preserve an indurated, wavy laminated or very thinly bedded calcrete horizon between 1.1 and 3.0 m beneath the profile top that ranges from 100 to 300 mm thick (e.g., Fig. 5). In several instances, vertically oriented carbonate tubules in overlying horizons become horizontally oriented upon entering the upper surface or within the calcrete layer (e.g., Fig. 5).

Type B paleosols have been described from the lower, middle and upper Moradi Formation, although examples with satin-spar cement textures are limited to the lower- and upper units. All of these blocky-structured mudstones overlie cross-bedded fine to medium

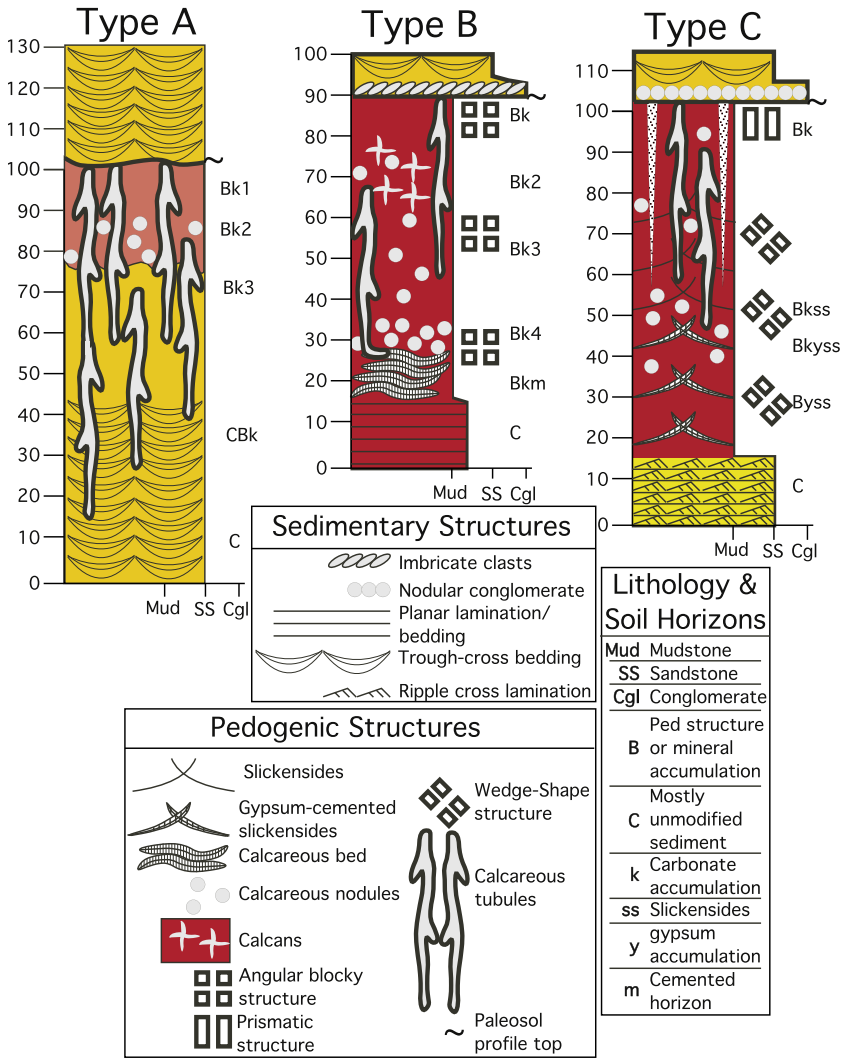


**Fig. 5.** Diagrams of paleosol types described from the upper Moradi Formation. Drawn here are: a Type A paleosol profile from Section 2 (stratigraphic position of 2MOR16, 17), a Type B paleosol profile from Section 1 (stratigraphic position of UMOR1-7), and a Type C paleosol profile Section 3 (stratigraphic position of MW20-25). Refer to Fig. 3 for the stratigraphic position of these profiles. Legend explains the icons and codes used to represent sedimentary and pedogenic structures, lithology and paleosol horizons. See text for further discussion.

sandstones, finely laminated siltstones or laminated mudstones and are overlain by either (1) bedded conglomeratic mudstones that do not appear to have scoured the upper surface of the paleosol profile or (2) trough cross-bedded sandstones which locally scour the upper surface of the profile (Figs. 3 and 5). Type B paleosols have been traced laterally for distances up to 0.9 km without any significant change in their overall morphology.

Petrographic inspection of Type B paleosol matrix reveals that micritic and microspar carbonate cements are concentrated upon the surfaces of fine to very fine mudstone blocks (e.g., Fig. 7D), but that micrite cement also becomes more diffuse toward the centers of the blocks. Carbonate nodules and tubules are composed of clotted, dark brown concentric rings of micritic calcite, some of which contain calcite-spar-filled septarian cracks. Silicic calcareous tubules and nodules are composed of length-slow chalcedony that has isomorphically replaced sparry calcite crystals (Fig. 7C). In addition, calcareous structures with satin-spar fabric are composed of fibrous carbonate bisected by a medial scar. In polarized light, the mudstone blocks are composed primarily of opaque clay-size material and silt-size quartz and feldspar grains that preserve Fe-oxide-rich crusts upon their exteriors (Fig. 7D).

X-ray powder diffraction peaks near 3.03 Å indicate that all carbonate in Type B paleosols is low-Mg calcite (e.g., Fig. 6B). X-ray diffraction spectra of oriented aggregates from the <2 μm fraction of all these mud-rich paleosol profiles include 10 Å peaks in all treatments, which corresponds to the d(001) peak of Illite (e.g., Fig. 6E). In addition, there is a 12 Å peak observed in <2 μm fraction samples after $K^+$ saturation at 25 °C which collapses to 10 Å after 2 h heating at 500 °C and a ~14.5 Å peak after $Mg^{2+}$ saturation that expands to ~18 Å after glycerol solvation (e.g., Fig. 6E). This behaviour indicates that the peak corresponds to the d(001) of smectite. One sample from the upper layer of a Type B paleosol (MW 30; Fig. 3) exhibits a broad and low ~7.2 Å peak with $K^+$ saturation that collapses after 2 h heating at 500 °C, which indicates the presence of kaolinite. Finally, a ~9.35 Å peak that is present in all treatments (Fig. 6E), which indicates the presence of talc ($Mg_3Si_4O_{10}(OH)_2$), occurs only in those Type B paleosols which also preserve satin-spar carbonate texture. However, the occurrence of talc within these profiles appears to be limited to discrete layers within the profiles, for example, 22–30 cm beneath the top of profile LMOR1-7, and in the upper 1.15 m of profile UMOR1-7 (Table 1).

### 4.3. Description of Type C paleosol morphology

Type C paleosols consist of 0.9 to 2.1 m thick weak red to red (Munsell Colors 10R4/3 to 10R 5/6) mudstone units that exhibit wedge-shape aggregate structures (Fig. 5) within layers interpreted

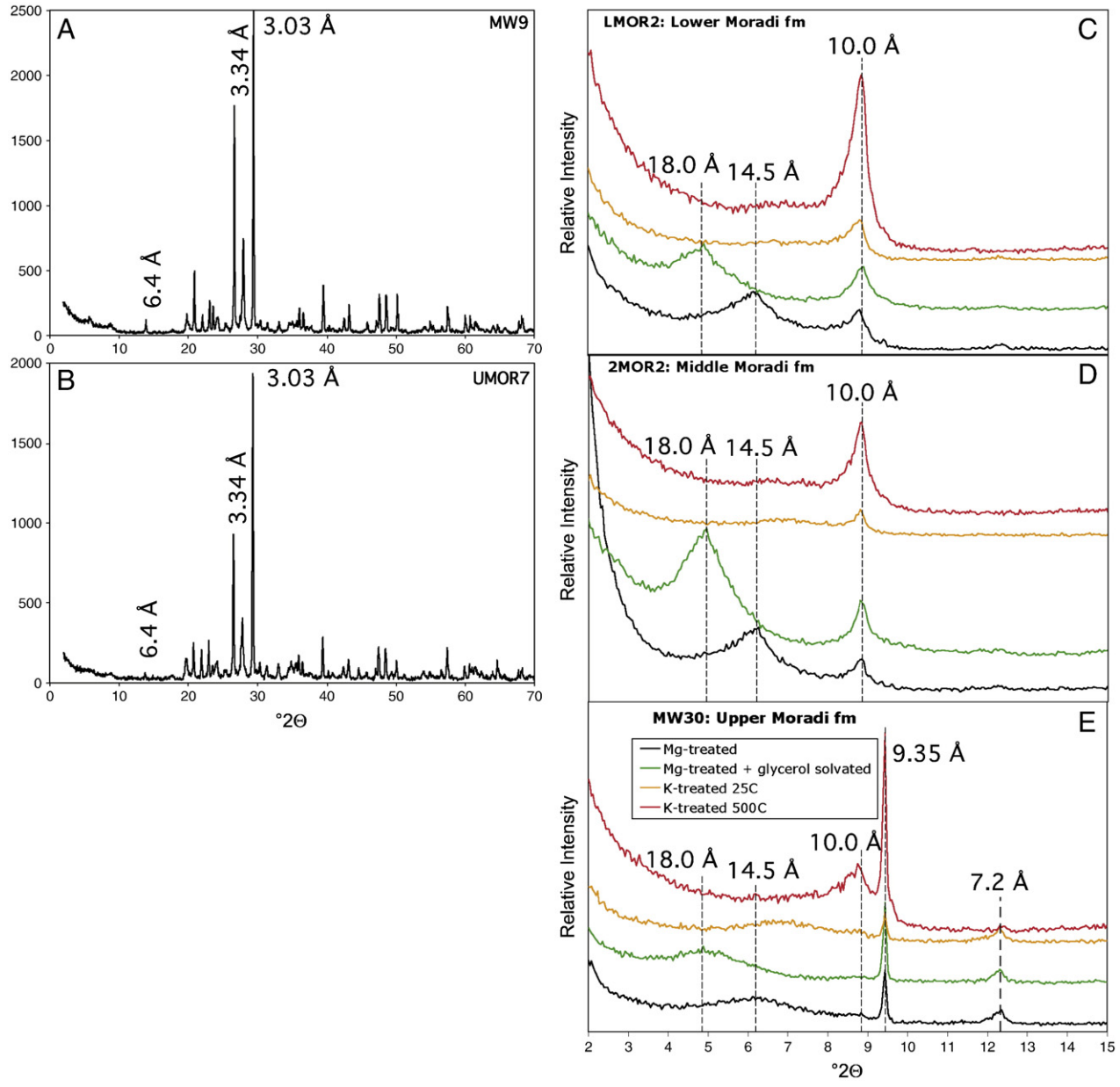


**Fig. 6.** X-ray diffractograms from paleosol samples collected in the Moradi Formation. (A) X-ray spectrum of a powder mount from a sandstone-dominated Type A paleosol that was sampled from Section 3, in the middle Moradi Formation, at the stratigraphic level of MW9 (see Fig. 3). (B) X-ray spectrum of a powder mount from a mudstone-dominated Type B paleosol that was sampled from Section 1, in the upper Moradi Formation, at the stratigraphic level of UMOR1-7 (see Fig. 3). (C) X-ray spectra from the <2 μm e.s.d. fraction of a Type B paleosol from Section 1, in the lower Moradi Formation, at the stratigraphic position of LMOR1-7. (D) X-ray spectra from the <2 μm e.s.d. fraction of a Type C paleosol from Section 2, in the upper Moradi Formation, at the stratigraphic position of 2MOR1-7. (E) X-ray spectra from the <2 μm e.s.d. fraction of a Type C paleosol from Section 3, in the upper Moradi Formation, at the stratigraphic position of MW30,31. For C–E, black line corresponds to $Mg^{2+}$-saturated samples, green line corresponds to $Mg^{2+}$-saturated and glycerol-solvated samples, orange line corresponds to $K^{+}$-saturated samples analyzed after drying at 25 °C, and red line corresponds to $K^{+}$-saturated samples analyzed after heating at 500 °C for 2 h. See text for discussion.

to have been subsurface B horizons. These wedge-shape aggregates are up to 300 mm wide and are bound by slickensides that define a wavy upper boundary within the soil profile. The mudstones above the wavy boundary are composed of medium and fine (5–20 mm) angular blocks and medium-sized (20–50 mm) prismatic blocks with secondary medium-sized angular blocky structure (Fig. 5). In addition, the upper blocky layers commonly exhibit vertically oriented silt- and sand-filled dikes that are as much as 40 mm wide at the top and taper downward to approximately 400 mm depth (Fig. 5). While the upper 150 to 300 mm of these profiles is noncalcareous, carbonate nodules and concretions ranging from a few mm to ~50 mm in diameter are common (5–20% by volume) to abundant (>20%) in lower layers, and they generally become larger downward. Two examples of Type C (2MOR1-7, MW21-25; Fig. 3) paleosols preserve calcareous cements with satin-spar fabric (similar to that observed in some Type B paleosols) along slickenplanes (Fig. 4D) and around platy structures beneath the horizons with slickensides. Type C paleosols are limited to upper Moradi Formation strata. They occur only within red mudstones and are commonly overlain by sandstones and conglomerates (e.g., Figs. 3 and 5) and have been traced laterally for distances up to 0.9 km without any significant change in their overall morphology.

Petrographic inspection of Type C paleosol matrix reveals the presence of carbonate-filled circumgranular cracks (Fig. 7D). Carbonate nodules are primarily composed of micrite, but also include microspar- and sparite-filled veins. Calcareous structures with satin-

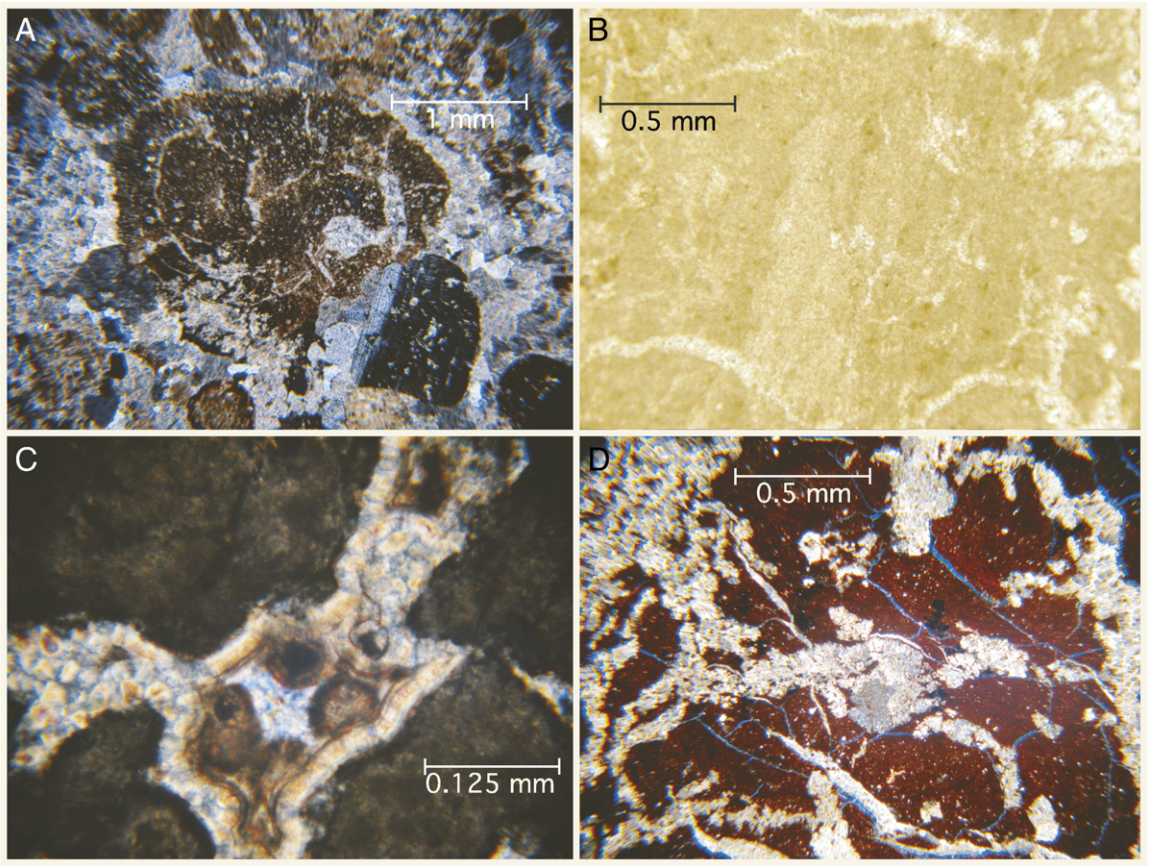


**Fig. 7.** Photomicrographs of Moradi Formation paleosols. (A) Photomicrograph of a rip-up mud-ball aggregate imaged with crossed nichols polarization from Section 2, in the middle Moradi Formation, at the stratigraphic level of 2MOR13 (see Fig. 3). (B) Plane-light photomicrograph of a calcareous tubule sampled from a Type A paleosol in Section 2, in the upper Moradi Formation, at the stratigraphic level of 2MOR15 (see Fig. 3). (C) Photomicrograph with crossed nichols polarization of length-slow chalcedony that has replaced pre-existing calcite spar in a calcareous tubule from a Type B paleosol in Section 3, in the upper Moradi Formation, at the stratigraphic level of MW39 (see Fig. 3). (D) Photomicrograph of microspar cements under crossed nichols polarization from a Type B paleosol in Section 1, in the upper Moradi Formation, at the stratigraphic level of UMOR1-7. See text for discussion.

**Table 1**
Mineralogy of <2 μm equivalent spherical diameter (e.s.d.) fraction from paleosols in the Moradi Fm.

| Sample | Section | Position in stratigraphy | Level (m) | Paleosol type | Mineralogy[a] |
|---|---|---|---|---|---|
| LMOR2 | 1 | Lower | N/A | B | Sm, Il |
| LMOR3 | 1 | Upper | N/A | B | Sm, Il |
| LMOR4 | 1 | Upper | N/A | B | Sm, Il |
| LMOR5 | 1 | Upper | N/A | B | Sm, Il |
| LMOR7 | 1 | Upper | N/A | B | Tal, Il, Sm |
| LMOR8 | 1 | Upper | N/A | B | Sm, Il |
| UMOR2 | 1 | Upper | 14.5 | B | Sm, Il |
| UMOR3 | 1 | Upper | 14.8 | B | Sm, Il, Tal |
| UMOR4 | 1 | Upper | 14.9 | B | Sm, Il, Tal |
| UMOR6 | 1 | Upper | 15.1 | B | Sm, Il, Tal |
| UMOR7 | 1 | Upper | 15.25 | B | Sm, Il, Tal |
| 2MOR1 | 1 | Upper | 0.1 | C | Sm, Il |
| 2MOR2 | 1 | Upper | 0.25 | C | Sm, Il |
| 2MOR3 | 2 | Upper | 0.35 | C | Sm, Il |
| 2MOR5 | 2 | Upper | 0.5 | C | Sm, Il |
| 2MOR6 | 2 | Upper | 0.7 | C | Sm, Il, Tal, K |
| Fossil1 | 3 | Upper | 40.1 | B | Sm, Il |
| MW17 | 3 | Upper | 50.1 | B | Sm, Il |
| MW21 | 3 | Upper | 64.3 | C | Sm, Il |
| MW22 | 3 | Upper | 64.5 | C | Sm, Il |
| MW23 | 3 | Upper | 64.6 | C | Sm, Il |
| MW25 | 3 | Upper | 64.7 | C | Tal, Sm, Il, K |
| MW30 | 3 | Upper | 81 | B | Tal, Sm, K |

[a] Sm = Smectite, Il = Illite; mica-like mineral, K = kaolinite, Tal = talc. The order of the reported clay minerals corresponds to decreasing values of area under the background subtracted X-ray diffraction peak for the d(001) reflection angle of the particular mineral, which is considered to be an approximation of relative amounts of the mineral within the sample.

spar fabric are composed of fibrous carbonate bisected by a medial scar. In polarized light, the mudstone blocks are composed primarily of opaque clay-size material and silt-size quartz and feldspar grains that preserve Fe-oxide-rich crusts upon their exteriors (Fig. 7D). X-ray powder diffraction peaks near 3.03 Å indicate that all carbonates in Type B paleosols are low-mg calcite (e.g., Fig. 6B). X-ray diffraction spectra of oriented aggregates from the <2 μm fraction of all these mud-rich paleosol profiles include 10 Å peaks in all treatments, which corresponds to the d(001) peak of Illite (e.g., Fig. 7B). In addition, there is a ~12 Å peak with $K^+$ saturation at 25 °C which collapses to 10 Å after 2 h at 500 °C and a ~14.5 Å peak with $Mg^{2+}$ saturation which expands to ~18 Å with $Mg^{2+}$ saturation and glycerol solvation (e.g., Fig. 7B) in all samples. This behavior indicates the presence of smectite in all Type C paleosols. Two samples (2MOR6, MW25), both from the upper 10 cm of Type C paleosols (Fig. 3) exhibit broad and low ~7.2 Å peaks with K + saturation that collapses after 2 h heating at 500 °C, which indicates the presence of kaolinite. Finally, the same two samples that contain kaolinite (2MOR6, MW25) also exhibit a ~9.35 Å peak in all treatments, which indicates the presence of talc.

## 5. Paleosol interpretation

Paleosol morphologies, mineralogy, petrographic textures and fabrics among the three different types of paleosols are used to classify each type of paleosol according to the paleosol taxonomy of Mack et al. (1993). For each paleosol type we also consider the closest estimated soil taxon within the context of the USDA Soil Classification System (Soil Survey Staff, 1975, 1996). Paleosols assigned to each

Order are interpreted as being the product of similar soil-forming environments in which local and regional processes combined to produce a distinctive weathering profile.

### 5.1. Paleosol morphology and petrography

The calcareous tubules observed in Type A, and calcareous tubules and vertically stacked nodules observed in Type B paleosol profiles, are interpreted to be rhizoliths. This interpretation reflects their morphological and mineralogical similarity to rhizoliths described from modern soils and paleosol occurrences elsewhere (e.g., Blodgett, 1988; Klappa, 1979, 1980; Loope, 1980; Smith, 1990). The discrete calcareous nodules and concretions that occur rarely in Type A, and commonly to abundantly in Type B and Type C paleosols, are interpreted to be equivalent to Machette's (1985) Stage II pedogenic carbonate accumulations resulting from translocation of $Ca^{2+}$ ion through the soil to the depth of wetting (Machette, 1985; McFadden and Tinsley, 1985). The sharp boundary between the carbonate cements and siliciclastic-rich paleosol matrix surrounding the nodules and concretions may arise from (1) fracturing of a pre-existing calcareous rhizolith in the soil and/or (3) reworking of the calcite cements through wetting–drying, and shrink–swell cycles, in the soil profiles (e.g., Brewer, 1976). Given that silica in the calcareous tubules and nodules from some Type B paleosols appears to isomorphically replace sparry calcite, and that sparry calcite is not typical of pedogenic carbonate (e.g., Deutz et al., 2001, 2002; Klappa, 1980; Wright, 1990), but rather appears to more commonly result from recrystallization of finer material after burial, we interpret the silica in these tubules to have replaced sparry calcite at some time after burial, and therefore the occurrence of silica within these paleosols offers no insights to Permian pedogenesis in the Tim Mersoi Basin.

The massive structure to highly disturbed sedimentary structure in Type A paleosols probably reflects its well-sorted sand parent lithology. Soil profiles dominated by detrital sands seldom exhibit soil structures because they lack the finely crystalline material, shrink–swell capacity, and cohesivity that is necessary to form well-developed peds (e.g., Buol et al., 1997). Pedogenesis in these sandy soil profiles characteristically obliterates primary sedimentary structures and develops the “single-grain structure” (Buol et al., 1997) or “massive” structure (Boggs, 2001). It is important to note, however, that single grain structure need not imply a short duration of pedogenesis (e.g., Choudhari, 2008; Hugget, 1998; Lichter, 1998), nor is what sedimentologists refer to as massive structure only formed by pedogenesis. The large volumes of pedogenic calcite that are locally concentrated in some Type A paleosol profiles suggests that pedogenesis may have persisted for hundreds or thousands of years (e.g., Gile, 1966; Machette, 1985). The blocky and prismatic mudstones in Type B and Type C paleosol profiles are interpreted to be pedogenically-produced structures that result from episodic wetting-and-drying, and corresponding volume changes of soil material under low confining pressure, whereas the wedge-shape aggregate structures, and slickenplanes defining them, are interpreted to have formed by repeated moisture-induced shrink–swell cycles under higher confining pressures (Buol et al., 1997; Schaetzel and Anderson, 2005).

Microcrystalline and microspar carbonate coatings of the ped surfaces are interpreted to be accumulations of calcite that formed during Permian soil formation. Similar structures, named “calcans” or “calcitans” (e.g., Brewer, 1976), form in modern soils with torric to aridic soil moistures regimes via translocation of $Ca^{2+}$ ion through the soil from weathering of primary minerals and dissolution of carbonate minerals in overlying horizons (McFadden and Tinsley, 1985). Torric and aridic soil moisture regimes correspond to soil profiles with a soil moisture control section (texturally dependent) that are (1) dry in all parts for more than half of the cumulative days per year when the soil temperature at depth of 50 cm from soil surface is above 5 °C; and (2) moist in some or all parts for less than 90 consecutive days when the soil temperature at a depth of 50 cm is above 8 °C (USDA Soil Taxonomy, 1975, 1996). Although petrography and XRD analysis of the carbonates with satin-spar texture in some Type B and Type C paleosols do not indicate the presence of gypsum, this fabric is one that is so characteristic of gypsum (e.g., Collins, 1984) that we interpret them to have been pedogenic gypsum that accumulated upon the surface of soil peds (gypsans; Brewer, 1976) and was subsequently isomorphically replaced by calcite some time after burial.

### 5.2. Clay mineralogy of Moradi Formation paleosol profiles

Moradi Formation paleosols contain the phyllosilicate minerals illite, smectite, kaolinite and talc. Illite is a common detrital mineral in sedimentary strata and is particularly common in soil profiles developed in alluvium (Southard and Miller, 1966; Yemane et al., 1996). Therefore, the illite in all the paleosol samples (Table 1) is probably inherited from the soil parent material. It is also possible for smectite to be inherited from the parent material (Southard and Miller, 1966; Wilson, 1999), but in this case it probably represents either a weathering product that formed from hydrolytic breakdown of primary minerals in the watershed or a pedogenic mineral that formed in-situ. Either way, the presence of smectite in Moradi Formation paleosol profiles is interpreted as indicative of poorly drained lowlands in the Tim Mersoi Basin under seasonal monsoonal climate. Smectite derived from weathering would indicate an environment with relatively low water:rock ratios and base-rich reactants which leads to favorable chemical conditions for smectite crystallization being high pH, high silica activity and an abundance of basic cations in solution.

Kaolinite may also be present in soil profiles as a result of inheritance from parent material (Southard and Miller, 1966). However, where present in the Moradi Formation, the kaolinite is limited only to the upper 30 cm of paleosol profiles, suggesting that it is somehow related to a pedogenic process. Soil profiles that are dominated by kaolinte in the phyllosilicate mineral fraction are typically associated with environments characterized by intense chemical weathering of soil materials in stable landscapes under warm, humid conditions (Wilson, 1999). Nevertheless, kaolinite may occur as an auxiliary phyllosilicate in the most intensively weathered upper layers of well-drained soil profiles in most climatic settings (Tabor et al., 2002; Yemane et al., 1996). Therefore, the occurrence of kaolinite in the horizons of Type B and Type C paleosols in the Moradi Formation is not surprising, and indicates well-drained conditions in some of the soils across some parts of the Tim Mersoi Basin during Permian time.

The occurrence of talc in these paleosols is unusual, as this mineral is typically associated with greenschist facies metamorphic terranes and hydrothermal alteration products along shear zones that develop in carbonate rocks (Friedman, 1965). Fluid inclusion studies indicate brine migration through parts of the Carboniferous strata in the Tim Mersoi Basin at temperatures ranging from 85 to 175 °C (Pagel et al., 2005), much lower than conditions necessary for greenschist-facies metamorphism. In addition, talc may occur as a detrital mineral in soil profiles (Léveillé et al., 2000; Singer, 1979). This possibility seems a reasonable explanation for the Moradi Formation paleosols, considering that the Aïr Mountains, a regional source of sediments for the Tim Masoi Basin, contains both talc and pyrophyllite (Davis, 1999). However, talc in the Moradi Formation is limited only to paleosol horizons with evidence for gypsum accumulation (as indicated by the presence of calcite with satin-spar texture) and its stratigraphic and spatial distribution in the Moradi Formation is too restricted to support a detrital origin. Therefore, we suspect the rare presence of talc in Moradi paleosols must be somehow related to pedogenesis.

Talc has never been demonstrated to be a direct product of pedogenesis (e.g., Wilson, 1999; but see also Noack et al., 1986). In

fact, stratiform talc occurrences are typically no younger than Paleozoic (Noack et al., 1986; but see also Bradley, 1964). Several spectroscopic and oxygen isotope studies of ancient stratiform talc indicate a low temperature (as low as 30–100 °C) origin that derives from diagenetic alteration of pre-existing Mg-rich phyllosilicate minerals (Bradley, 1964; Noack et al., 1986) such as sepiolite ($Mg_4Si_6O_{15}(OH)_2{\bullet}6H_2O$), stevensite ($((Ca,Mg)_XMg_6Si_8O_{20}(OH)_4{\bullet}nH_2O$), saponite ($Na_{0.3}Mg_3(SiAl_4O_{10}(OH)_2{\bullet}nH_2O)$) or possibly palygorskite ($(Mg,Al)_5(Si,Al)_8O_{20}(OH)_2{\bullet}8H_2O$, all of which have been reported as authigenic minerals in modern aridosols characterized by highly saline soil solutions with a pH >8.5 (e.g., Calvo et al., 1999; Wilson, 1999). We think this scenario best explains the occurrence of talc in the Moradi Formation paleosol profiles, because (1) the co-occurrence of talc with satin-spar calcite textures, a likely replacement of original pedogenic gypsum, is suggestive of saline soil solutions and (2) pedogenic calcite in the profiles indicates alkaline solution pH (>8) that likely would have been conducive to crystallization of Mg-rich phyllosilicates, which (3) encountered appropriate burial temperatures for diagenetic transformation to talc. Therefore, we interpret talc in the Moradi Formation paleosol profiles to be a diagenetic alteration product of a Mg-rich phyllosilicate (probably sepiolite). Furthermore, considering the distribution of modern soils that contain Mg-rich phyllosilicates, we interpret those Type B and Type C paleosol profiles that contain talc to have undergone pedogenesis in an arid to hyper-arid climate.

### 5.3. Type A paleosol classification and environmental interpretation

Considering their lack of soil structure and evidence for pedogenic carbonate accumulation around rooting structures, Type A paleosol profiles are classified as calcic Protosols (Mack et al., 1993) and roughly correspond to the range of characteristics observed in the USDA Soil Taxonomy soil orders Entisols and some suborders of Inceptisols and Aridisols (Soil Survey Staff, 1996). The distribution of Protosols in the Moradi Formation indicates that sedimentation within these parts of the basin ceased long enough for colonization by terrestrial flora (Buol et al., 1997). This terrestrial flora presumably allowed, in turn, for colonization by a tetrapod fauna (e.g., Sidor et al., 2005).

The close association of the calcic Protosols with well-sorted, trough-cross bedded sandstone (e.g., Figs. 3 and 4A) suggests that these soils developed within abandoned or ephemeral fluvial channels which may have been subject to scour and burial during infrequent flash-flood episodes. This “flashy” flow hypothesis is also suggested by the taphonomy of the Moradi fauna: fifteen disarticulated skeletons of large herbivourous reptiles (belonging to the endemic pareiasaur *Bunostegos*) dip gently towards a channel axis and may have been deposited with sediments from an ephemeral flash flood (Smith et al., 2009).

Soil development in such unstable parts of the landscape has been documented in ephemeral, anabranching river systems in modern-day northeastern semi-arid (Fielding and Alexander, 2001), and central arid (Tooth and Nanson, 2000) regions of Australia. In both instances, strongly seasonal distribution of precipitation causes extreme variations in river flow. Extended periods of minimal flow permit specialized woody trees to colonize and mature within the channel as clusters or groves. This life habit (1) enhances the ability of the grove to withstand periodic inundation by high-energy flows (2) permits phreatophytes in extremely arid climates to take advantage of the most readily available, and often most shallow, source of fresh water that flows through the sandy channel-fill sediments (Camporeale et al., 2006; Laity, 2007), and (3) when the river is aggrading its bed, it enhances the preservation potential of root systems. Similar paleosol profiles that preserve calcareous rhizoliths in fluvial channel sandstones and siltstones have been described from Lower and Upper Permian strata of Australia (Fielding and Alexander, 2001), Lower Permian strata of Utah (Tabor et al., 2007), and Upper Triassic strata of Argentina (Tabor et al., 2006). Based upon analogous modern soils, we herein interpret calcic Protosols in the Moradi Formation to represent soil formation within the channels of an ephemeral fluvial system characterized by long-term low-flow conditions.

### 5.4. Type B paleosol classification and environmental interpretation

The abundance of carbonate in Type B paleosols, in conjunction with well-developed pedogenic structure, indicates they are Calcisols, whereas profiles that also preserve satin-spar gypsum textures between peds are classified as gypsic Calcisols (Mack et al., 1993). Similar morphologies in the USDA Soil Taxonomy occur within the soil Orders Inceptisols, Mollisols and Aridisols (Soil Survey Staff, 1996). The most important pedogenic process in the formation of Type B paleosols is the accumulation of carbonate minerals, which occurs when meteoric precipitation which percolates through the soil is substantially less than soil moisture removed via evapotranspiration (e.g., Arkley, 1963; Jenny, 1941), and is typical of regions characterized by low annual rainfall. For example, carbonate is not commonly precipitated in soil profiles with mean annual rainfall in excess of ~750 mm/year (Royer, 1999), whereas gypsum is not retained in the soil profile if rainfall exceeds ~300 mm/year (Watson, 1992).

The position of the laminated- to thinly-bedded calcrete horizons near the base of some Type B paleosol profiles (e.g., Fig. 5), in conjunction with a change in the orientation of rhizoliths from vertical above, to horizontal upon or within, the calcrete horizons suggests that these calcretes accumulated along the boundary of the phreatic and vadose environments. We interpret these basal calcrete horizons to provide an approximate position of the groundwater table for most of the year, and therefore conclude that the local to regional groundwater was quite shallow, commonly less than a meter beneath the land surface, over large areas of the Tim Mersoi Basin during Mid to Late Permian times. Modern soils of Australia and southern Africa forming in arid climates with a relatively shallow water table (<5 m) develop a similar calcareous B horizon (e.g. Semeniuk, 1981, 1985; Watson, 1992).

Calcisols and their modern soil equivalents represent relatively long intervals of stability upon the landscape, because significant amounts of time are required to translocate $Ca^{2+}$ ion, and accumulate carbonate, in silicate-hosted soils (e.g., Gile, 1966; Machette, 1985). The presence of nodular calcite in these paleosols suggests long periods of pedogenesis (between 1000 and 10,000 years) in areas of the flood plain removed from frequent overbank deposition (Gile et al., 1981). As such, Type B paleosols are interpreted to represent relatively old soils that were spatially removed from the depositional effects of major rivers and streams. In addition, the morphology of these profiles, in conjunction with mineralogical evidence for pedogenic Mg-phyllosilicates within them, suggests that they likely formed under semi-arid or hyper-arid climatic conditions, within a well-drained part of the basin yet with a relatively shallow groundwater system such as may be found on the slightly elevated interfluves that ran parallel to the major river channels.

### 5.5. Type C paleosol classification and environmental interpretation

The abundance of shrink–swell and desiccation features, in conjunction with the presence of calcite nodules in the subsurface horizons of Type C paleosols indicates they are calcic Vertisols (Mack et al., 1993). Alternatively, the profile that also preserved evidence for gypsum accumulation may be classified as gypsic calcic Vertisols (Mack et al., 1993). Similar morphologies in the USDA Soil Taxonomy occur within the soil Order Vertisols. In spite of the specific classification used for these paleosols, the dominant pedogenic process in the formation of Vertisols is shrinking and swelling of expansible 2:1 phyllosilicate clays (i.e., smectite) through repeated wetting and drying cycles in climates with seasonal precipitation and/

or fluctuating water table (Wilding and Tessier, 1988). Therefore, it is likely that Type C paleosols underwent seasonal episodic wetting and drying from flooding and/or heavy precipitation.

While pedogenic carbonate accumulation in most soil types corresponds to relatively low mean annual rainfall (e.g., ~750 mm/year; Royer, 1999), Vertisols appear to retain carbonate in the soil profile under considerably greater mean annual rainfall (~1500 mm/year; Nordt et al., 2006) due to the very high concentration of base cations, and $Ca^{2+}$ in particular, in these profiles. Furthermore, the presence of nodular calcite in these paleosols suggests long periods of pedogenesis (between 1000 and 10,000 years) in areas of the flood plain removed from frequent overbank or eolian deposition (Gile et al., 1981) such as on the plains surrounding playas or sabkhas. In addition, given the presence of calcite nodules, the possibility of pedogenic gypsum accumulation and mineralogical evidence for pedogenic mg-phyllosilicate in the upper layers of these paleosols, we interpret these profiles to have likely formed under semi-arid to hyperarid climatic conditions characterized by strongly seasonal monsoonal rainfall.

## 6. Summary and conclusions

Paleosol profiles in the Middle–Upper Permian Moradi Formation of the Tim Mersoi Basin, Niger include (1) calcic Protosols, (2) Calcisols and gypsic Calcisols, and (3) calcic Vertisols and gypsic calcic Vertisols. As mentioned earlier, each of these paleosol morphologies, and their mineralogy, provide persuasive evidence for pedogenesis under dry, semi-arid to hyper-arid climate. Comparison of the pedogenic gypsum and mg-phyllosilcates within the Moradi paleosol profiles with similar modern soil profiles in arid zones of Australia and southern Africa indicate precipitation was likely less than 300 mm/year (e.g., Calvo et al., 1999; Watson, 1992). Furthermore, based upon the spatial and stratigraphic distribution of paleosol profiles, there is little evidence for any significant shifts from “arid” in the overall climate history of the Moradi succession.

Significantly, the paleogeographic position upon which the Tim Mersoi Basin resided during Permian time is suspected to have been among the driest on the Pangean landmass as a result of a powerful southern-hemisphere monsoon circulation (the “Megamonsoon”; Kutzbach and Gallimore, 1989; Parrish, 1993; Peyser and Poulsen, 2008). General circulation models also predict that Permian climate over the Tim Mersoi Basin was characterized by extreme seasonality in rainfall (Gibbs et al., 2002; Patzkowsy et al., 1991), and was among the driest (<100 mm/year precipitation) and hottest (30–35 °C mean annual temperature) landscapes on Pangea (Peyser and Poulsen, 2008; Poulsen et al., 2007; see also Fig. 8). Our paleoclimatic interpretation of Moradi paleosols is generally consistent with environmental predictions from these conceptual and quantitative climate models. However, the current database of climate-sensitive lithologies and paleosol morphologies from the Moradi Formation presented herein is qualitative, and we are not able to quantify with precision from these indicators just how dry the landscapes of the Tim Mersoi Basin were in the Mid- to Late Permian.

Morphological variability of soils across the arid Moradi landscape are most likely attributed to conditions other than regional climate change, such as differences in lithology of the alluvium, and depth of the groundwater table beneath the surface. Both these factors are influenced by position in the basin and proximity to the axial drainage system.

Sedimentary facies within the Moradi Formation include (1) minor coarse-grained pebbly sandstones, conglomerates and breccias deposited on alluvial fans, (2) common fluvial channel sandstones deposited in axial rivers, (3) common mudrock-dominated floodplain and crevasse splay sequences (4) rare playa mudstones with laminated carbonates and (5) rare eolian sand dunes (Joulia, 1959; Wright et al., 1993). Our recent fieldwork suggests that only facies

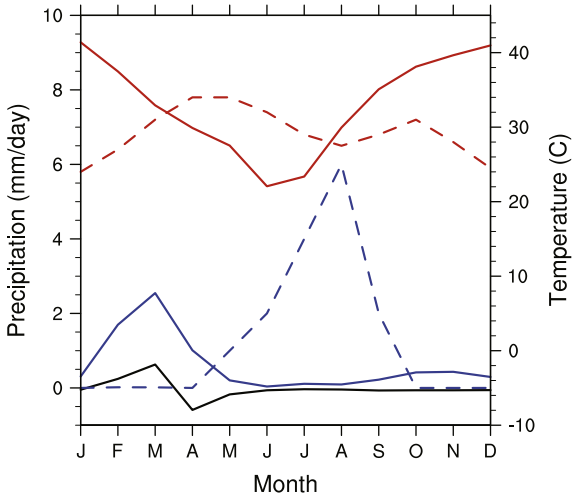


**Fig. 8.** Plot of rainfall (blue lines) and temperature (red lines) versus month over northern Niger as predicted from recently published results from recent general circulation models for Permian time (Poulsen et al., 2007; Peyser and Poulsen, 2008; solid lines) and historical synoptic data (dashed lines). This comparison shows that modern northern Niger receives substantially greater annual rainfall than that predicted for Permian time. This comparison also highlights differences in the seasonality of rainfall and temperature between modern and Permian northern Niger, which is attributed primarily to the paleogeographic position, ~20° south of the paleoequator, during Permian time. Model-based estimates of Permian precipitation–evapotraspiration suggest this region was among the most arid upon Permian Earth. See Text.

(1) through (4) are represented among the three stratigraphic sections, and only facies (1) through (3) preserve paleosol profiles.

Based upon the sporadic distribution of calcareous root structures and their preferred vertical orientation in the upper horizons of the Type A calcic Protosols which are closely associated with well-sorted trough cross-bedded sandstone, these rhizolith concentrations are interpreted to represent groves of phreatophytic trees and shrubs that grew within anabranching ephemeral stream channels. We consider these paleosols and their host channels to have been the main, albeit ephemeral, conduits of hydrological flow and sediment transport through the Tim Mersoi Basin during the Permian.

Type B Calcisols and gypsic Calcisols developed within fine-grained sediments, and development of angular blocky to prismatic structure, calcans, gypsans, and stacked carbonate nodules indicate these paleosols were mature, well-drained, soils that were distant from depocenters such as the ephemeral streams and lakes. We consider these paleosols and their host deposits to have developed upon slightly elevated interfluvial plains that were above the direct influence of the regional water table. However, the evidence for groundwater calcretes at the bases of some of these Type B paleosols suggests that groundwater was at times quite shallow; between 1 and 2.5 m beneath the soil surfaces.

Type C calcic Vertisols and gypsic calcic Vertisols developed within fine-grained sediments as well, but abundant evidence for shrink–swell structures in these paleosol profiles suggests that they were, at least seasonally, more poorly drained than Calcisols and gypsic Calcisols forming within the same basin. We consider this difference in paleosol structure, and the perceived difference in drainage, to indicate that Vertisols occupied a lower, more poorly drained position on the landscape including interfluvial plains proximal to ephemeral streams and areas surrounding ephemeral water bodies such as playas and possibly sabkhas.

A remarkable aspect of the paleosol profiles from the Moradi Formation is that, in spite of abundant proxy data for an arid climate, there is also a significant amount of proxy data to indicate that water was available in abundance, at least intermittently, in ephemeral

streams, shallow groundwater reservoirs and ephemeral lakes. Fossil amphibians from the Moradi Formation (e.g., the temnospondyls *Saharastega* and *Nigerpeton*) likely colonized these ephemeral water sources, as they depended on water for reproduction, as do modern frogs living in northern (arid) Niger today (e.g., Rödel, 2000).

These conditions are similar to those of the "wet desert" deposits in the Permian northern hemisphere in Europe (Brookfield, 2000; Frederiksen et al., 1998). It is reassuring that like the work presented herein, Brookfield (2000) also used the modern environments of Death Valley, California as a close modern analogue to support that study's interpretation of a Permian "wet desert" in Scotland.

## Acknowledgements

We are indebted to the Niger Ministry of Mines and Energy (Niamey, Niger) for access to the field sites and permitting the collection of samples for laboratory analysis. We thank Stephanie Thomas (SMU) for assistance in the field. Mary Milleson (SMU) helped with X-ray diffraction analyses of clay samples. Professor Finn Surlyk served as editor for this manuscript, and Professors Steven Driese (Baylor University) and Paul McCarthy (University of Alaska Fairbanks) reviewed an earlier version of this manuscript. This project was supported by the National Science Foundation grant NSF-EAR 0617250 to N.J. Tabor and C.A. Sidor as well as NSF-EAR 0545654 to N.J. Tabor and C.J. Poulsen.

## References

Arkley, R.J., 1963. Calculation of carbonate and water movement in soil from climatic data. Soil Science 96, 239–248.
Blakey, R.C., 2007. Carboniferous–Permian palaeogeography of the Assembly of Pangae. In: Wong, Th.E. (Ed.), Proceedings of the XVth International Congress on Carboniferous and Permian Stratigraphy. Utrecht, 10–16 August 2003. Royal Dutch Academy of Arts and Sciences, (Amsterdam), pp. 443–456.
Blodgett, R.H., 1988. Calcareous paleosols in the Triassic Dolores Formation, southwestern Colorado. Geological Society of America Special Paper 216, 103–121.
Boggs Jr., S., 2001. Principles of Sedimentology and Stratigraphy, 3rd Ed. Prentice Hall, New Jersey, U.S.A.. 726 pp.
Bradley, W.H., 1964. Lazurite, talc and chlorite in the Green River Formation of Wyoming. American Mineralogist 49, 881–887.
Brewer, R., 1976. Fabric and Mineral Analysis of Soils. Krieger, New York. 482 pp.
Brookfield, M.E., 2000. Temporary desert lake deposits, Lower Permian (Rotliegendes) Southern Scotland, U.K. In: Gierlowski-Kordesch, E.H., Kelts, K.R. (Eds.), Lake Basins Through Space and Time: AAPG Studies in Geology, 46, pp. 67–74.
Buol, S.W., Hole, F.D., McCracken, R.J., Southard, R.J., 1997. Soil Genesis and Classification. Iowa State University Press, Ames, IA. 527 pp.
Calvo, J.P., Blanc-Valleron, M.M., Rodriguez-Arandia, J.P., Rouchy, J.M., Sanz, M.E., 1999. Authigenic clay minerals in continental evaporitic environments. Special Publications of the International Association of Sedimentologists 27, 129–151.
Camporeale, C., Perona, P., Ridolfi, L., 2006. Hydrological and geomorphological significance of riparian vegetation in arid lands. In: Odorico, P.D., Porporato, A. (Eds.), Dryland Ecohydrology, pp. 161–179.
Choudhari, J.S., 2008. Relationship between pedogenetic manifestations in some arid soil and age of the landforms. Journal of Earth System Science 96, 203–210.
Collins, E.W., 1984. Styles of Deformation in Permian strata, Texas Panhandle. Bureau of Economic Geology Geological Circular 84-4, Austin, U.S.A. 32 pp.
Davis, E.A., 1999. Metamorphosis in the culture market of Niger. American Anthropologist 101, 485–501.
Deutz, P., Montañez, I.P., Monger, H.C., Morrison, J., 2001. Derivation of a palaeoenvironmental record from pedogenic carbonates in buried and relict Quaternary soils, Rio Grande Rift, New Mexico. Palaeogeography, Palaeoclimatology, Palaeoecology 166, 293–317.
Deutz, P., Montañez, I.P., Monger, H.C., 2002. Morphology and stable and radiogenic isotope composition of pedogenic carbonate in late Quaternary relict soils, New Mexico: an integrated record of pedogenic overprinting. Journal of Sedimentary Research 72, 809–822.
DiMichele, W.A., Montanez, I.P., Poulsen, C.J., Tabor, N.J., 2009. Climate and vegetational regime shifts in the late Paleozoic ice age earth. Geobiology 7, 200–226.
Fielding, C.R., Alexander, J., 2001. Fossil trees in ancient fluvial channel deposits: evidence of seasonal and longer-term climatic stability. Palaeogeography, Palaeoclimatology, Palaeoecology 170, 59–80.
Fielding, C.R., Frank, T.D., Birgenheier, L.P., Rygel, M.C., Jones, A.T., Roberts, J., 2008. Stratigraphic imprint of the Late Palaeozoic ice age in eastern Australia: a record of alternating glacial and nonglacial climate regime. Journal of the Geological Society of London 165, 129–140.
Frederiksen, K.S., Clemmensen, L.B., Lawaetz, H.S., 1998. Sequential architecture and cyclicity in Permian desert deposits, Brodick Beds, Arran, Scotland. Journal of the Geological Society 155, 677–683.
Friedman, G.M., 1965. Occurrence of talc as a clay mineral in sedimentary rocks. Nature 207, 283–284.
Gibbs, M.T., Rees, P.M., Kutzbach, J.E., Ziegler, A.M., Behling, P.J., Rowley, D.B., 2002. Simulations of Permian climate and comparisons with climate-sensitive sediments. Journal of Geology 110, 33–55.
Gile, L.H., 1966. Morphological and genetic sequences of carbonate accumulation in desert soils. Soil Science 101, 347–360.
Gile, L.H., Hawley, J.W., Grossman, R.B., 1981. Soils and geomorphology in the Basin and Range area of southern New Mexico. Guidebook to the Desert Project: New Mexico Bureau of Mines and Mineral Resources Memoir 39. 222 pp.
Greigert, J., Pougnet, R., 1967. Essai de description des formations géologiques de la République du Niger. Editions du Bureau de Recherches Géologiques et Minières, Paris. 273 pp.
Hugget, R.J., 1998. Soil chronosequences, soil development, and soil evolution: a critical review. Catena 32, 155–172.
Isbell, J.L., Miller, M.F., Wolfe, K.L., Lenaker, P.A., 2003. Timing of the late Palaeozoic glaciation in Gondwana: was glaciation responsible for the development of northern hemisphere cyclothems? In: Chan, M.A., Archer, A.W. (Eds.), Extreme Depositional Environments: Mega End Members in Geologic Time: Geological Society of America Special Paper, vol. 370, pp. 5–24.
JCPDS International Centre for Diffraction Data, 1980. Mineral Powder Diffraction File Data Book. JCPDS, Swarthmore, Pennsylvania USA. 1168 pp.
Jenny, H., 1941. Factors of Soil Formation. Dover Publications, Minneola, New York. 281 pp.
Joulia, F., 1959. Les Séries primaires au N et au NW de l'Aïr (Sahara central). Discordances observées. Bulletin de la Societe Geologique de France 7, 192–196.
Klappa, C.F., 1979. Calcified filaments in Quaternary calcretes; organo-mineral interactions in the subaerial vadose environment. Journal of Sedimentary Research 49, 955–968.
Klappa, C.F., 1980. Rhizoliths in terrestrial carbonates: classification, recognition, genesis and significance. Sedimentology 27, 613–629.
Kogbe, C.A., 1981. Cretaceous and Tertiary of the Iullemeden Basin in Niger (West Africa). Cretaceous Research 2, 129–186.
Kutzbach, J.E., Gallimore, R.G., 1989. Pangean climates: megamonsoons of the megacontinent. Journal of Geophysical Research 94, 3341–3357.
Laity, J., 2007. Aeolian destabilization along the Mojave River, Mojave desert, California: linkages among fluvial, groundwater, and aeolian systems. Physical Geography 24, 196–221.
Léveillé, R.J., Fyfe, W.S., Longstaffe, F.J., 2000. Unusual secondary Ca–Mg–Carbonate–Kerolite deposits in basaltic caves, Kauai, Hawaii. Journal of Geology 108, 613–621.
Lichter, J., 1998. Rates of weathering and chemical depletion in soils across a chronosequence of Lake Michigan sand dunes. Geoderma 85, 255–282.
Loope, D.B., 1980. Evidence for soil-forming episodes during deposition of the Permian Cedar Mesa Sandstone of Utah. Geological Society of America Abstracts with Program 12, 278.
Lucas, S.G., 2004. A global hiatus in the Middle Permian tetrapod fossil record. Stratigraphy 1, 47–64.
Nairn, A.E.M., Smithwick, M.E., 1976. Permian palaeogeography and climatology. In: Falke, H. (Ed.), The Continental Permian in Central,West, and South Europe. D. Reidel, Boston, pp. 283–312.
Machette, M.N., 1985. Calcic soils the Southwestern United States. Geological Society of America Special Paper 203, 1–22.
Mack, G.H., James, W.C., Monger, H.C., 1993. Classification of paleosols. Geological Society of America Bulletin 105, 129–136.
McFadden, L.D., Tinsley, J.C., 1985. Rate and depth of pedogenic–carbonate accumulation in soils: formulation and testing of a compartment model. Geological Society of America Special Paper 203, 23–42.
Ministère des Mines et de l'Hydraulique, Direction des Mines et de la Géologie. 1977. Afasto, Carte Géologique Echelle 1:200,000 Notice Explicative.
Moore, R.C., Reynolds, R.J., 1997. X-ray Diffraction and the Identification and Analysis of Clay Minerals. Oxford University Press. 296 pp.
Newell, A.J., Tverokhlebov, V.P., Benton, M.J., 1999. Interplay of tectonics and climate on a transverse fluvial system, Upper Permian, Southern Uralian Foreland Basin, Russia. Sedimentary Geology 127, 11–29.
Noack, Y., Decarreau, A., Manceau, A., 1986. Spectroscopic and oxygen isotopic evidence for low and high-temperature origin of talc. Bulletin of Mineralogy 109, 253–263.
Nordt, L., Orosz, M., Driese, S., Tubbs, J., 2006. Vertisol carbonate properties in relation to mean annual precipitation: implications for paleoprecipitation estimates. Journal of Geology 114, 501–510.
Pagel, M., Cavellec, S., Forbes, P., Gerbaud, O., Vergely, P., Wagani, I., 2005. Uranium deposits in the Arlit area (Niger). In: Mao, J., Bierlein, M.P. (Eds.), Mineral Deposit Research, Meeting the Global Challenge, Proceedings of the 8th SGA Meeting in Beijing, China. Society for Geology Applied to Mineral Deposits, Switzerland, pp. 303–305.
Parrish, 1982. Upwelling and petroleum source beds, with reference to the Palaeozoic. Bull. Am. Assoc. Pet. Geol. 66, 750–774.
Parrish, J.T., 1993. Climate of the supercontinent Pangaea. J. Geol. 101, 215–233.
Patzkowsy, M.E., Smith, L.H., Markwick, P.J., Engberts, C.J., Gyllenhaal, E.D., 1991. Application of the Fujita–Ziegler Palaeoclimate Model: Early Permian and Late Cretaceous examples. Palaeogeography, Palaeoclimatology, Palaeoecology 86, 67–85.
Peyser, C.E., Poulsen, C.J., 2008. Controls on Permo-Carboniferous precipitation over tropical Pangaea: a GCM sensitivity study. Palaeogeography, Palaeoclimatology, Palaeoecology 268, 181–192.
Poulsen, C.J., Pollard, D., Montañez, I.P., Rowley, D., 2007. Late Palaeozoic tropical climate response to Gondwana deglaciation. Geology 35, 771–774.

Rees, P.M., Ziegler, A.M., Gibbs, M.T., Kutzbach, J.E., Behling, P.J., Rowley, D.B., 2002. Phytogeographic patterns and climate data/model comparisons. Journal of Geology 110, 1–31.
Retallack, G.J., Smith, R.M.H., Ward, P.D., 2003. Vertebrate extinction across Permian–Triassic boundary in Karoo Basin, South Africa. Geological Society of America Bulletin 115, 1133–1152.
Ricardi-Branco, F., 2008. Venezuelan paleoflora of the Pennsylvanian–Early Permian: paleobiogeographical relationships to central and western equatorial Pangea. Gondwana Research 14, 297–305.
Rödel, M.O., 2000. Herptofauna of West Africa, Volume 1: Amphibians of the West African Savana. Chimaira, Frankfurt. 335 pp.
Royer, D.L., 1999. Depth to pedogenic carbonate horizon as a paleoprecipitation indicator? Geology 27, 1123–1126.
Schaetzel, R.J., Anderson, S., 2005. Soils; Genesis and Geomorphology. Cambridge University Press, New York. 817 pp.
Schneider, J.W., Korner, F., Roscher, M., Kroner, U., 2006. Permian climate development in the northern peri-Tehys area—Lodève basin, French Masif Central, compared in a European and Global context. Palaeogeography, Palaeoclimatology, Palaeoecology 243, 92–117.
Scotese, C.R., Boucot, A.J., McKerrow, W.S., 1999. Gondwanan palaeogeography and palaeoclimatology. Journal of African Earth Sciences 28, 99–114.
Semeniuk, V., 1981. Calcrete in Quaternary coastal dunes in southwestern Australia: a capillary-rise phenomenon associated with plants. Journal of Sedimentary Petrology 51, 47–68.
Semeniuk, V., 1985. Distribution of calcrete in Holocene coastal sands in relationship to climate, southwestern Australia. Journal of Sedimentary Petrology 55, 86–95.
Sidor, C.A., O'Keefe, F.R., Damiani, R., Steyer, J.S., Smith, R.M.H., Larson, H.C.E., Sereno, P.C., Ide, O., Maga, A., 2005. Permian tetrapods from the Sahara show climate-controlled endemism in Pangea. Nature 434, 886–889.
Singer, A., 1979. Palygorskite in sediments: detrital, diagenetic and neoformed — a critical review. Geologische Rundschau 68, 996–1008.
Smith, R.M.H., 1990. Alluvial paleosols and pedofacies sequences in the Permian Lower Beaufort of the southwestern Karoo basin, South Africa. Journal of Sedimentary Research 60, 258–276.
Smith, R.M.H., Sidor, C.A., Tabor, N.J., Steyer, J.S., Chaney, D.S., 2009. Vertebrate taphonomy and ichnology of a Permian 'wet desert' in central Pangea. Palaeontologia Africana 44, 179–183.
Soil Survey Staff, 1975. Soil Taxonomy. US Department of Agriculture Handbook, p. 436. 754 pp.
Soil Survey Staff, 1996. Keys to Soil Taxonomy, 7th Ed. USDA, Natural Resources Conservation Service, Washington, DC. 332 pp.
Southard, A.R., Miller, R.W., 1966. Parent material–clay relations in some northern Utah soils. Proceedings — Soil Science Society of America Journal 30, 97–101.
Steel, R.J., 1974. Cornstone (fossil caliche) — its origin, stratigraphic, and sedimentological importance in the New Red Sandstone, Western Scotland. Journal of Geology 82, 351–369.
Tabor, N.J., Montañez, I.P., 2004. Permo-Pennsylvanian alluvial paleosols (north-central Texas): high-resolution proxy records of the evolution of early Pangean paleoclimate. Sedimentology 51, 851–884.
Tabor, N.J., Montanez, I.P., Southard, R.J., 2002. Paleoenvironmental reconstruction from chemical and isotopic compositions of Permo-Pennsylvanian pedogenic minerals. Geochimica et Cosmochimica Acta 66, 3093–3107.
Tabor, N.J., Montanez, I.P., Kelso, K.A., Currie, B.S., Shippman, T.A., 2006. A Late Triassic soil catena: landscape controls on paleosol morphology across the Carnian-Age Ischigualasto-Villa Union Basin, Northwestern Argentina. In: Alonso-Zarza, A.M., Tanner, L.H. (Eds.), Paleoenvironmental Record and Applications of Calcretes and Palustrine Carbonates: Geological Society of America Special Paper, 416, pp. 17–41.
Tabor, N.J., Montanez, I.P., Steiner, M., Schwindt, D., 2007. The $\delta^{13}C$ values of Permo-Triassic carbonates from South Africa reflect a stinking, sulfurous swamp, not atmospheric conditions: Palaeogeography, Palaeoclimatology, Palaeoecology 252, 370–381.
Taquet, P., 1969. Première découverte en Afrique d'un reptile captorhinomorphe (coylosaurien). Comptes Rendus de l'Académie des Science, Paris, Série D 268, 779–781.
Taquet, P., 1972. Un exemple de datation et de corrélation stratigraphique basé sur les Captorhinomorphes (Reptiles cotylosauriens). Mémoirs du Bureau de Recherches Géologiques et Minières 77, 407–409.
Tooth, S., Nanson, G.C., 2000. The role of vegetation in the formation of anabranching channels in an ephemeral river, northern plains, arid central Australia. Hydrological Processes 14, 3099–3117.
Tramp, K.L., Soreghan, G.S., Elmore, R.D., 2004. Palaeoclimatic inferences from palaeopedology and magnetism of the Permian Maroon Formation loessite, Colorado, USA. Geological Society of America Bulletin 116, 671–686.
Trompette, R., Affaton, P., Joulia, F., Marchand, J., 1980. Stratigraphic and structural controls of late Precambrian phosphate deposits of the northern Volta Basin in the upper Volta, Niger, and Benin, West Africa. Economic Geology 75, 62–70.
Watson, A., 1992. Desert soils. Developments in Earth Surface Processes, vol. 2. Elsevier, New York, pp. 225–260.
Wilding, L.P., Tessier, D., 1988. Genesis of vertisols: shrink-swell phenomena. In: Wilding, L.P., Puentes, R. (Eds.), Vertisols: Their Distribution, Properties, Classification and Management. Texas A&M University Publishing Center, College Station, TX, pp. 55–81.
Wilson, M.J., 1999. The origin and formation of clay minerals in soils: past, present and future perspectives. Clay Minerals 34, 7–25.
Wopfner, H., 2002. Tectonic and climatic events controlling deposition in Tanzanian Karoo basins. Journal of African Earth Sciences 34, 167–177.
Wopfner, H., Kreuser, T., 1986. Evidence for Late Palaeozoic glaciation in southern Tanzania. Palaeogeography, Palaeoclimatology, Palaeoecology 56, 275–295.
Wright, V.P., 1990. A micromorphological classification of fossil and recent calcic and petrocalcic microstructures. In: Douglas, L.A. (Ed.), Soil Micromorphology: A Basic and Applied Science. Elsevier, Amsterdam, pp. 401–407.
Wright, L.I., Branchet, M., Alisso, I., 1993. Notice explicative de la Carte Géologique au 1/50.000 du basin Houiller D'Anou-Araren/Solomi. Ministère des Mines et de l'Energie, République du Niger. 20 pp.
Yakimenko, E., Inozemtsev, S., Naugolnykh, S., 2004. Upper Permian paleosols (Salarevskian Formation) in the central part of the Russian Platform: paleoecology and paleoenvironment. Revista Mexicana de Ciencias Geologicas 21, 110–119.
Yemane, K., Kahr, G., Kelts, K., 1996. Imprints of postglacial climates and paleogeography in the detrital clay mineral assemblages of an Upper Permian fluviolacustrine Gondwana deposit from north-central Malawi. Palaeogeography, Palaeoclimatology, Palaeoecology 125, 27–49.
Ziegler, A.M., Hulver, M.L., Rowley, D.B., 1997. Permian world topography and climate. In: Martini, I.P. (Ed.), Late Glacial and Post-Glacial Environmental Changes — Quaternary, Carboniferous–Permian and Proterozoic. Oxford University Press, Oxford, pp. 111–146.
Ziegler, A.M., Eshel, G., Rees, P.McA., Rothfus, T.A., Rowley, D.B., Sunderlin, D., 2003. Tracing the tropics across land and sea: Permian to present. Lethaia 36, 227–254.